Reduced Order Based Compensator Control of Thin Film Growth in a CVD Reactor

H.T. Banks and H.T. Tran

Abstract. This paper reports on an interdisciplinary effort, which involves applied mathematicians, material scientists and physicists at North Carolina State University, to integrate new intelligent processing approaches with advanced mathematical modeling, optimization, and control theory to guide the construction and experimental implementation of a series of high pressure (up to 100 atm) organometallic chemical vapor deposition (CVD) reactors. An integral component of this research program is the design of the reactor so that control and sensing are a basic component of the optimal design efforts for the reactor. We report here on the successful use of mathematics in a fundamental role in the development of linear and nonlinear feedback control methods for real-time implementation on the reactor. This is achieved in the required context of gas dynamics coupled with nonlinear surface deposition processes. The problems are optimal tracking problems (for the chemical component fluxes over the substrate) that employ state-dependent Riccati gains with nonlinear observations and the resulting dual state dependent Riccati equations for the compensator gains. This control methodology is successfully combined with reduced order model methods based on proper orthogonal decomposition techniques. Computational results to support the efficacy of our approach and methods are also included.

1. Introduction

Chemical vapor deposition (CVD) is an important industrial technique used to grow thin films with certain desired properties. This process involves the deposition of precursor vapor sources onto a heated substrate where they react to form the desired material. CVD is a key element in a wide variety of advanced industrial applications, ranging from the development of short wavelength light sources to detectors and integrated sensors, in particular the integration of III-V optoelectronics and silicon technology. In addition, wide bandgap materials are of particular interest for advanced silicon ULSI technology in the context of dielectric isolation, vertical integration, optically interconnected common memory, integrated sensors and microwave applications. These materials are also of considerable interest in the context of optoelectronics for applications in displays, optical recording, signal

processing, printing and medicine [1]. In these processes, the control of the concentrations and distributions of both point defects and extended defects and the related control of the surface morphology and interfacial chemistry for compound semiconductor heterostructures are essential because of their important role in the control of the electrical/optical properties and the reliability of wide bandgap semiconductor devices and circuits.

For the past five years, an interdisciplinary effort at North Carolina State University has been carried out to explore new intelligent processing approaches that access conditions outside the capabilities of conventional methods. Generally the control of the stoichiometry, and the related issue of the control of the point defect chemistry of the heteroepitaxial layers of mixed III-V compounds requires, under the conditions of thermally activated growth, high ratios in the fluxes of the group V to the group III source materials. In this context we have explored organometallic CVD (OMCVD) under superatmospheric conditions (up to 100 atm), where high partial pressure ratios can be established without compromise with respect to the growth rate. Because the process is operating at high flows/vapor densities, control of the fluid dynamics becomes essential for optimal growth conditions. Therefore advanced methods of mathematical modeling, optimization, and control theory have been applied to guide the development and experimental implementation of these processes. In particular, advanced simulations for flow processes in a computer-aided design (CAD) mode resulted in several generations of reactor geometries before a suitable configuration that promised desirable flow characteristics near the substrate was obtained. In this presentation we discuss a third generation reactor design (see Fig. 1) resulting from this developmental process. For a fourth generation reactor design see [23].

The mathematical models for OMCVD (under superatmospheric pressure) possess one of the most complex fluid dynamics systems imaginable. Some of the complex issues in computing chemically reacting flows include the simulation of three-dimensional flows governed by Navier-Stokes equation coupled with equations for energy and species and strong temperature dependence of the physical properties of gases. Chemical reactions are taking place in the gas-phase as well as on the substrate. However, since only a trace amount of reactants mixed with carrier gas is used, a dilute approximation is assumed. This leads to a quasi-steady gas-phase model with steady-state nonlinear coupled system of equations for the continuity, momentum and energy that is decoupled from the time dependent species equations. This gas phase model is coupled with a reduced order model of the surface reactions involved in the decomposition of source vapors from the gas phase and the growing film on the substrate.

The resulting mathematical model is a system of partial differential equations coupled with nonlinear ordinary differential equations describing the surface deposition process. Numerical simulations and control designs and syntheses of such systems are faced with considerable challenges regarding dimensionality and nonlinearity. This paper describes our efforts during the last five years to overcome

these difficulties. More specifically, §2 describes the proper orthogonal decomposition (POD) technique, also known as the Karhunen-Loève procedure, that is used to obtain low dimensional dynamic models of distributed parameter systems. The POD method, which is well known in statistical and pattern recognition fields [2], has been shown to be an effective tool for the analysis of complex systems such as turbulence flows, shear flows, and weather prediction (see e.g., [3] and the references therein). Roughly speaking, POD is an optimal technique of finding a basis that spans an ensemble of data, collected from an experiment or a numerical simulation of a dynamical system, in the sense that when these basis functions are used in a Galerkin procedure, they will yield a finite dimensional system with the smallest possible degrees of freedom. Thus this method may well be suited to treat optimal control and parameter estimation of distributed parameter systems. In §3, we describe our successful use of POD techniques as a reduced basis method for computation of feedback controls and compensators in a high pressure CVD reactor. More specifically, we present a proof-of-concept computational implementation of this method with a simplified growth example of group III-V compounds that includes multiple species and controls, gas phase reactions (no surface reactions), and time dependent tracking signals that are consistent with pulsed vapor reactant inputs. In §4 state estimation and feedback tracking control methods for nonlinear systems are presented. The methods, which are based on the "state-dependent Riccati equations", allow the construction of nonlinear estimators and nonlinear feedback tracking controls for a wide class of systems including high pressure CVD systems considered here. The performance of the nonlinear estimator and tracking control will be presented on a flight dynamics simulation example. Finally, §5 contains our overall conclusions.

2. Proper Orthogonal Decomposition

In general, the discretization of linear/nonlinear partial differential equations using finite element, finite volume, or finite different methods involves basis functions that have little to do with the differential equation. For example, piecewise polynomials are used in the finite element method, grid functions are used in the finite difference method, and Legendre or Chebyshev polynomials are used in some spectral methods. POD, on the other hand, uses basis functions that span a data set, collected from an experiment or numerical simulation of a dynamical system, in a certain "optimal" fashion. Because POD basis elements are optimal in the sense that they are the extractions of characteristic features of the data set, frequently only a small number of POD basis functions are needed to describe the solution. POD based approximation methods have been applied to numerous applications including turbulent coherent flows [4], shear flows [5], characterization of human faces [6], and image recognition [7]. More recently, the possibility of POD based control design and parameter estimation has been proposed. In particular, applications of POD to optimization or open loop control were developed in [8, 9, 10],

to feedback control design were reported in [11, 12, 13, 14, 15], and to parameter estimation or inverse problems were discussed in [16]. References to recent work of other authors can be found in [11]-[16] and [23].

We now outline an algorithm to obtain the POD basis element. The mathematical basis for the algorithm has been described in numerous articles (see e.g., [8]). Let $\{\mathbf{U}_i(\vec{x}) : 1 \leq i \leq N; \vec{x} \in \Omega\}$ denote the set of N observations (also called *snapshots*) of some physical processes over a domain Ω. In the context of CVD process, these observations could be experimental measurements or numerical solutions of velocity fields, temperatures, species etc. taken at different physical parameters (Reynolds number, input flow rates etc.) or time steps.

Step 1. *Compute the covariant matrix* $\mathbf{C}$. The matrix elements of $\mathbf{C}$ are given by

$$\mathbf{C}_{ik} = \frac{1}{N} \int_\Omega \mathbf{U}_i(\vec{x}) \mathbf{U}_k(\vec{x}) d\vec{x},$$

for $i, k = 1, 2, \ldots, N$.

Step 2. *Solve the eigenvalue problem* $\mathbf{CV} = \lambda \mathbf{V}$. Since $\mathbf{C}$ is a nonnegative, Hermitian matrix, it has a complete set of orthogonal eigenvectors

$$\mathbf{V}^1 = \begin{bmatrix} a_1^1 \\ a_2^1 \\ \vdots \\ a_N^1 \end{bmatrix}, \mathbf{V}^2 = \begin{bmatrix} a_1^2 \\ a_2^2 \\ \vdots \\ a_N^2 \end{bmatrix}, \ldots, \mathbf{V}^N = \begin{bmatrix} a_1^N \\ a_2^N \\ \vdots \\ a_N^N \end{bmatrix}$$

with the corresponding eigenvalues arranged in ascending order as $\lambda_1 \geq \lambda_2 \geq \cdots \geq \lambda_N \geq 0$.

Step 3. *Compute the POD basis vectors.* The POD basis elements $\Phi_i(\vec{x})$ such that $X^{\text{POD}} = \text{span}\{\Phi_1, \Phi_2, \ldots, \Phi_N\}$, where X^{POD} is the finite-dimensional POD space, are given as

$$\Phi_k = \sum_{i=1}^N a_i^k \mathbf{U}_i,$$

where $1 \leq k \leq N$ and a_i^k are the elements of the eigenvector $\mathbf{V}^k$ corresponding to the eigenvalue λ_k.

To approximate a distributed parameter system by a finite-dimensional problem one uses a combination of Galerkin procedures and POD basis elements (see [11, 12] for details). However, to this point we have not discussed any model reduction features associated with using POD basis elements in approximation schemes. In the algorithm described above, the number N may be large, $100 - 1000$ or even more, depending on the complexity of the dynamics represented in the "snapshots" $\mathbf{U}_i$. In general, one should take N sufficiently large so that the snapshots $\mathbf{U}_i$ contain all salient features of the dynamics being investigated. Thus, the POD basis functions Φ_i, used with the original dynamics in a Galerkin procedure, offers the possibilities of achieving a high fidelity model, albeit with perhaps a large dimension N.

To achieve model reduction, one chooses $M \ll N$ and carries out a Galerkin procedure with the set of elements $\{\Phi_1, \Phi_2, \ldots, \Phi_M\}$. The crucial question is how to choose M. As discussed elsewhere (see e.g., [11, 12]) the percentage of the total snapshots set data variability contained in a certain POD mode Φ_k is given by the ratio of the eigenvalue λ_k to the total of all eigenvalues, $\lambda_k / \sum_{j=1}^{N} \lambda_j$. The reason for ordering the POD modes from highest to lowest eigenvalues is to include as much of the variability of the system into the first few modes as possible. Therefore to capture most of the data variability of the system contained in the N POD elements, it suffices to choose M, where M is sufficiently smaller than N, so that $\sum_{i=1}^{M} \lambda_i \approx \sum_{i=1}^{N} \lambda_i$. For the CVD examples studied in [8, 11, 12], the POD system was constructed for $N = 100 - 200$ and a reduced order model with $M = 2 - 10$ resulted in a truly significant computational savings.

While the above comments suggest the proper choice for the dimension of the reduced order model to be used in simulations, there are additional order questions related to the linear control system to be used in determining reduced order gains and compensators. We have found that the ranks of the controllability and observability matrices have sometimes been useful criteria (see the discussion in [13, 11, 12]) to help in the choice of the number of modes to use in control design applications for the reduced basis representation.

In the next section, we present a proof-of-concept computational implementation of this method with a simplified growth example for III-V layers. In this example we implement Dirichlet boundary control of dilute reactants transported by convection and diffusion to an absorbing substrate after they undergo gas phase reactions.

3. Application of POD to Compensator Control of CVD

The particular geometry of the differentially pressure controlled (DPC) reactor system under consideration here features horizontal flow of the process gases and source vapor/carrier gas mixtures into an expansion section leading into a rectangular channel that contains the substrate (see Fig. 1). The substrate wafer is mounted on a rotating induction heated SiC coated graphite susceptor. The exhaust gases are vented through a vertical exhaust tube. Loading and unloading of substrate wafers is accomplished through a load-lock chamber beneath the radio frequency (rf) section of the reactor that can be evacuated by a turbomolecular pump. After purging with ultra-pure nitrogen, sample transfer can be executed using a magnetic transfer rod. Gas is purging through the gap between the susceptor and the reactor's base to avoid flow of gas mixtures to the mechanical workings behind the susceptor. The quartz glass reactor is connected at the inlet to a source vapor/process gas flow control and switching panel that directs individual streams of source vapor saturated carrier gas either to a vent line or to the reactor. Thus, pulsed operation separating plugs of source vapor saturated carrier gas by plugs of

high purity carrier gas, flow rate modulated flow or continuous flow can be implemented for all source vapors without change in reactor pressure or total flow. Two optical windows at the Brewster angle of the substrate are attached to the sides of the reactor. They allow for the real-time process monitoring utilizing p-polarized reflectance spectroscopy (PRS) (see e.g., [17] and the references therein).

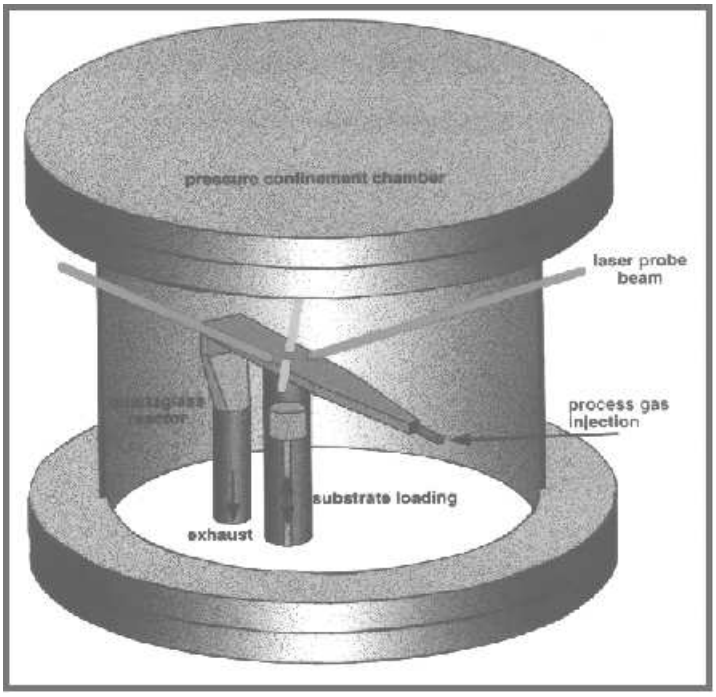

FIGURE 1. Schematic representation of a horizontal, quartz reactor in a steel confinement shell

To demonstrate the feasibility of using POD technique as a reduced basis method for computation of feedback controls and compensators in a high pressure CVD reactor, we will restrict our study to a two-dimensional rectangular domain (Fig. 2) representing the longitudinal cross section through the center of the reactor. We consider the deposition of InP using pulsed trimethyl-indium (TMI) and phosphine (PH_3) as source vapors and hydrogen as carrier gas. In particular, at first only carrier gas flows through the reactor. After the flow reaches steady state, a pulse of reactant (e.g., TMI) diluted with carrier gas enters the reactor. After the pulse, the reactor is then flushed with carrier gas. This process is then repeated for another reactant. Pulsing of the III-V source materials prevents nucleation of the film in the gas phase and make PRS observation and analysis possible.

We consider only trace amounts of reactants mixed with the carrier gas. Under this dilute approximation, we can classify CVD processes as a quasi-transient

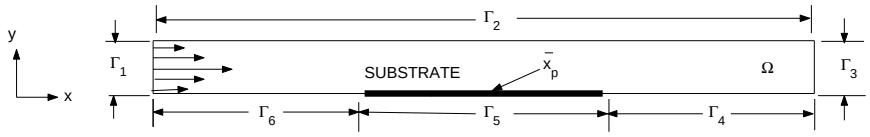

FIGURE 2. Two-dimensional cross section of the CVD reactor (height=0.011m, length=0.156m, substrate length=0.048m)

flow (steady-state flow with transient species). The steady-state flow is described by the following set of equations [12]
(continuity)

$$\vec{\nabla} \cdot (\rho \vec{v}) = 0, \tag{1}$$

(momentum)

$$\rho \vec{v} \cdot \vec{\nabla} \vec{v} = -\vec{\nabla} P + \vec{\nabla} \cdot \vec{\tau} - \rho \vec{g}, \tag{2}$$

where the viscous stress tensor is of the form

$$\vec{\tau} = -\frac{2}{3}\mu(\vec{\nabla} \cdot \vec{v})\vec{I} + \mu(\vec{\nabla}\vec{v} + \vec{\nabla}\vec{v}^T), \tag{3}$$

(energy)

$$\rho c_p \vec{v} \cdot \vec{\nabla} T = \vec{\nabla} \cdot (k \vec{\nabla} T), \tag{4}$$

where $\vec{g}$ is the gravitational acceleration, $\vec{u}$, T, and P are the velocity, temperature, and pressure, μ, c_p, and k are the viscosity, specific heat, and thermal conductivity of the carrier gas. The density variations are modeled as [12]

$$\rho = \rho_0[1 - \beta(T - T_0)], \tag{5}$$

where T_0 is a reference temperature, ρ_0 is a reference density calculated from the ideal gas law at the reference temperature and reactor pressure, and β is the volume coefficient of expansion ($\beta = 1/T$). In addition, we consider a hydrogen carrier gas at atmospheric pressure. Temperature dependent values for μ, k, and c_p are linearly interpolated from measurements taken from the available literature [12]. A parabolic velocity flow profile is specified at the inlet ($\Gamma 1$), with an average inlet velocity of 0.1147 m/s. No slip (zero velocity) boundary conditions are imposed on those portions of the model corresponding to the reactor walls ($\Gamma 2, \Gamma 4, \Gamma 5$, and $\Gamma 6$). Room temperature boundary conditions are imposed at the inlet and along the upper wall ($\Gamma 2$). Along the bottom wall, the substrate ($\Gamma 5$) temperature is fixed at 800°K , with a non-linear temperature decrease from the substrate edge

to the inlet ($\Gamma 6$) and, similarly, from the substrate edge to the outlet ($\Gamma 4$) (see Fig. 2).

Steady-state solutions for v, T, and ρ obtained from equations (1-4) are then used in the time-dependent species equations for the precursor mass fractions [12],

$$\frac{\partial Y_n}{\partial t} + \vec{v} \cdot \vec{\nabla} Y_n = \frac{1}{\rho} \vec{\nabla} \cdot \left(\rho D_n \vec{\nabla} Y_n \right) + \sum_{i=1}^{N_R} r_{ni} \, , \tag{6}$$

where D_n is the diffusivity of the species, Y_n is the mass fraction of the nth species, N_R is the number of gas phase reactions, and r_{ni} is the rate of production of species n in the ith chemical reaction.

Under the reactor conditions considered here (H_2 carrier gas, 800°K substrate temperature, and 1 atm pressure), there are no effective gas phase reaction mechanisms for phosphine, and the only significant gas phase reaction for TMI is the decomposition of TMI to MonoMethylIndium (MMI) and two methyl molecules, $In(CH_3)_3 \rightarrow InCH_3 + 2CH_3$. This reaction can be described as a first-order Arrhenius reaction [12]

$$r_n = \nu_n \frac{W_n}{W_{\rm TMI}} k_0 e^{(-E/RT)} Y_{\rm TMI}, \tag{7}$$

where ν_n refers to the stoichiometry of species n in the reaction, W_n and $W_{\rm TMI}$ refer to the molecular weight of species n and TMI, respectively, $k_0 = 5.25 \times 10^{15}$ s^{-1} is the rate constant, and $E = 47.2$ kcal/mol is the activation energy [18].

The tracking control problem that we formulate is to find the mass fractions of TMI and phosphine at the inlet (Γ_1) of the reactor in order to obtain a desired flux $q_T(t)$ of reactants at point $\vec{x}_p$ on the susceptor (Γ_5). That is, we consider to minimize a cost functional of the form

$$J(u) = \int_0^\infty \left[u' R u + (q - q_T)' Q (q - q_T) \right] dt, \tag{8}$$

subject to

$$\begin{array}{rcll}
\frac{\partial Y_n}{\partial t} + \vec{v} \cdot \vec{\nabla} Y_n & = & \frac{1}{\rho} \vec{\nabla} \cdot \left(\rho D_n \vec{\nabla} Y_n \right) + \lambda_n Y_1 & \\
Y_n(0, \vec{x}) & = & y_{n0}(\vec{x}) & \\
Y_1(t, \vec{x}) & = & u_1(t) & \text{on } \Gamma 1 \\
Y_2(t, \vec{x}) & = & u_2(t) & \text{on } \Gamma 1 \\
Y_3(t, \vec{x}) & = & 0 & \text{on } \Gamma 1 \\
Y_n(t, \vec{x}) & = & 0 & \text{on } \Gamma 5 \\
\frac{\partial Y_n(t, \vec{x})}{\partial n} & = & 0 & \text{on } \Gamma 2 \cup \Gamma 3 \cup \Gamma 4 \cup \Gamma 6 \\
n & = & 1, 2, 3, &
\end{array} \tag{9}$$

where Y_1, Y_2, and Y_3 refer to the mass fractions of TMI, phosphine, and MMI, respectively; $u_1(t), u_2(t)$ are the controls corresponding to TMI and phosphine; $\lambda_1(T) = -k_0 e^{(-E/RT)}$, $\lambda_2(T) = 0$, and $\lambda_3(T) = (W_3/W_1) k_0 e^{(-E/RT)}$; $\vec{v}$, ρ, T are the steady state solutions to equations (1-4); and $\frac{\partial}{\partial n}$ denotes the outward normal

derivative. Finally, the general flux vector, $q(t)$, at the point $\vec{x}_p$ is given by

$$q(t) = \begin{bmatrix} q_{\rm In}(t) \\ q_P(t) \end{bmatrix} = -\rho \begin{bmatrix} D_1 \frac{W_{\rm In}}{W_1} \left.\frac{\partial Y_1}{\partial n}\right|_{\vec{x}_p} + D_3 \frac{W_{\rm In}}{W_3} \left.\frac{\partial Y_3}{\partial n}\right|_{\vec{x}_p} \\ D_2 \frac{W_P}{W_2} \left.\frac{\partial Y_2}{\partial n}\right|_{\vec{x}_p} \end{bmatrix}, \tag{10}$$

where $W_{\rm In}$ and W_P are the molecular weights of indium (a component of Y_1 and Y_3) and phosphorus (Y_2), respectively.

We note that since the methyl (CH_3) molecules do not participate in film growth or otherwise affect the transport properties (under the dilute approximation), we do not include them in the state equations (9). The reactor walls ($\Gamma 2$, $\Gamma 4$, and $\Gamma 6$) are assumed non-absorbing, and the substrate ($\Gamma 5$) is assumed to be perfectly absorbing (concentration of zero). Temperature dependent values for the diffusivities D_n in hydrogen are linearly interpolated from values taken from the available literature [18].

We next use a penalty boundary formulation on the species state equations (9) to change all Dirichlet boundary conditions to Neumann conditions. For example, the Dirichlet condition $Y_1(t,\vec{x}) = u_1(t)$ is reformulated as $\frac{\partial Y_1(t,\vec{x})}{\partial n} = \frac{1}{\epsilon}(Y_1(t,\vec{x}) - u_1(t))$, where ϵ is a small parameter (for most of our calculations we used $\epsilon = 10^{-3}$). This boundary conditions reformulation provides a natural setting for the Galerkin procedure as well as for the control formulation. More specifically, writing the state equation in weak form using test function w_j, integrate by parts, and applying the modified Newmann conditions, we obtain

$$\begin{aligned} \int_\Omega \tfrac{\partial Y_n}{\partial t} w_j \, d\Omega \;\; = \;\; & -\int_\Omega \left(\vec{v}\cdot\vec{\nabla}Y_n\right) w_j \, d\Omega - \int_\Omega D_n \vec{\nabla} Y_n \cdot \vec{\nabla} w_j \, d\Omega \\ & + \int_\Omega \tfrac{1}{\rho} w_j D_n \vec{\nabla} Y_n \cdot \vec{\nabla}\rho \, d\Omega + \int_\Omega \lambda_n Y_n w_j \, d\Omega \\ & + \tfrac{1}{\epsilon}\int_{\Gamma 1,\Gamma 5} w_j D_n Y_n \, ds - \tfrac{1}{\epsilon}\int_{\Gamma 1} w_j D_n u_n \, ds \;, \end{aligned} \tag{11}$$

where $n = 1, 2, 3$ and $u_3 \equiv 0$. The mass fraction of the nth species is approximated as a linear combination of the M_n most significant POD basis elements as

$$Y_n^{M_n}(t,\vec{x}) = \sum_{i=1}^{M_n} y_{n,i}(t)\Phi_{n,i}(\vec{x}), \tag{12}$$

where $M_n \ll N$ and $\Phi_{n,i}$ is the ith POD basis element corresponding to the nth species. Using the representation (12) and the orthonormality of the $\{\Phi\}'s$, we apply a Galerkin procedure to the weak form (11) to obtain a system of M ordinary differential equations for the coefficients $y_{n,i}$

$$\dot{y}^M(t) = A^M y^M(t) + B^M u(t), \quad u(t) = \begin{bmatrix} u_1(t) \\ u_2(t) \end{bmatrix}, \tag{13}$$

where $M = \sum_{n=1}^{3} M_n$, A^M is an $M \times M$ matrix, and B^M is an $M \times 2$ matrix.

We remark that the POD modes for each species are constructed from 150 snapshots ($N = 150$) taken during the three second cycle (2 s pulsing, 1 s clearing) of each source species. Each solution vector represents the species mass fraction at the 453 nodal points and corresponds to a time increment of 0.03-s in the time range from 0 to 3 seconds. However, for the reduced order model, we used only

19 POD modes ($M = 19$: $M_{\text{TMI}} = 8$, $M_{\text{Phospine}} = 8$, $M_{\text{MMI}} = 3$), which yield a worst captured variability of 99.995% for MMI ($\sum_{j=1}^{3} \lambda_{\text{MMI}_j} / \sum_{k=1}^{150} \lambda_{\text{MMI}_k} = 99.995$). While the captured variability suggests the proper order for accurate reduced order model simulations, there are additional order questions related to the control system to be used in determining reduced order gains and compensators. For example, the ranks of the controllability and observability matrices have sometimes been found to be useful criteria to help in the choice of the number of modes to use in control design applications for the reduced basis representation [11, 12].

The reduced order species state model (13) is linear in both the state and control variables and, therefore, linear control methodologies can be applied to obtain the optimal feedback tracking control. However, the application of this feedback control to the reduced order model requires a linear state estimator since only partial state observations of the fluxes of In and P at the substrate center are available. These partial state observations are compatible with current PRS sensing technology. For detailed calculations of the POD basis elements, the reduced order model, and the compensator-based optimal feedback tracking control see the recent article [12].

To show how well the control/compensator system designed above via the reduced order model performs when used in the actual physical experiments, we computationally test the reduced order control/compensator design on the full system, which is approximated by 453×3 quadratic finite elements. We emphasize that the reduced order model is formulated using only 19 POD basis elements, a substantial order reduction from 453×3. Fig. 3 depicts plots of the observed fluxes as functions of time. It clearly shows that the system is able to closely track the time dependence of the desired flux profile (shown in dotted line) without significant delays. It also confirms that the ability of the system to match the target flux is sensitive to the design parameter Q.

4. Nonlinear Tracking Control and State Estimator

4.1. Tracking Control for Nonlinear Systems

In general, the mathematical model developed in §3 has to be linked with a surface kinetics model describing the decomposition kinetics of the organometallic precursors involved and their incorporation into the film deposition. For the growth of epitaxial GaP heterostructures on Si(001) substrates, a reduced order surface kinetics (ROSK) model is proposed in [19]. This surface kinetics model is a nonlinear system of ordinary differential equations and when combining with the gas phase model will yield a system of nonlinear differential equations. In this section, we summarize our development of nonlinear estimators and nonlinear feedback tracking controls that are applicable to a wide class of systems including the high pressure CVD systems as considered here [20].

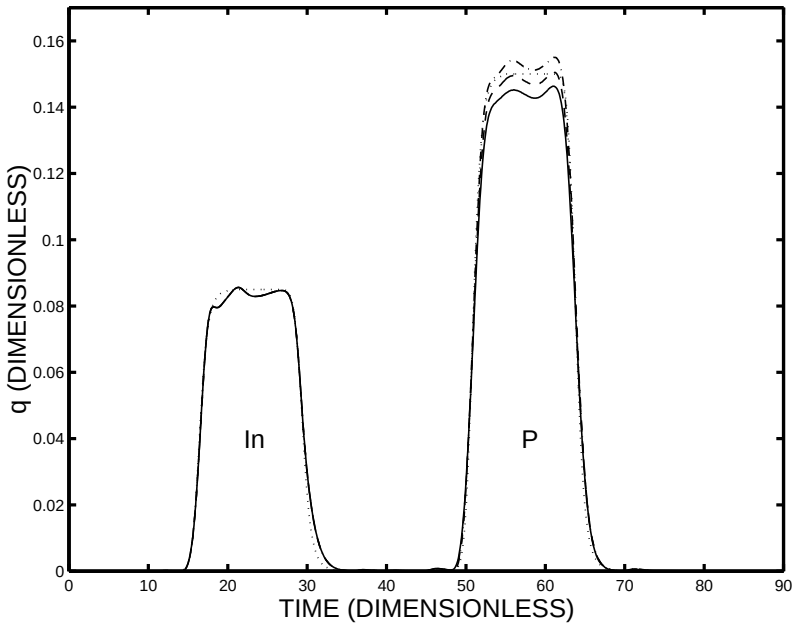

FIGURE 3. Observed fluxes as a function of time for different values of the control parameter Q: small (solid line), medium (dashed line), and large (dash-dot line). The target flux profile is also shown (dotted line) for reference. The system is able to closely track the desired flux profile.

Consider the following nonlinear control system

$$\begin{cases} \dot{x}(t) &= f(x(t)) + Bu(x(t),t) \\ x(0) &= x_0 \\ y(t) &= Hx(t), \end{cases}$$

where, for this presentation, the tracking variable y is taking to be a linear function of the state variables (see [20] for the nonlinear tracking variable case). In addition to the nonlinear state equation, the cost function for the tracking problem, with a desired trajectory $r(t)$, is given by

$$J(x_0, u) = \frac{1}{2}\int_0^\infty \left((y-r)^T Q(y-r) + u^T Ru\right) dt.$$

Now rewriting the nonlinear function as $f(x) = A(x)x$ and solving the necessary optimality conditions, we obtain the optimal feedback control

$$u(x,t) = -R^{-1}B^T\left[\Pi\left(x(t)\right)x(t) + s(t,x)\right], \tag{14}$$

where $\Pi(x)$ is the solution to the so-called state dependent Riccati equation (SDRE)

$$\Pi(x)A(x) + A^T(x)\Pi(x) - \Pi(x)BR^{-1}B^T\Pi(x) + H^TQH = 0 \tag{15}$$

and $s(t,x)$ is the solution to the following two-point boundary value problem

$$\begin{cases} \dot{s} &= -A^T(x_{nom})s + \Pi(x_{nom})BR^{-1}B^Ts + H^TQr \\ & \quad - \sum_{i=1}^m (x_{nom})_i \left(\frac{\partial A_{1\to m,i}}{\partial x_{nom}}(x_{nom})\right)^T (\Pi(x_{nom})x_{nom} + s) \\ & \quad - D_t\Pi(x_{nom})x_{nom} \\ \dot{x}_{nom} &= A(x_{nom})x_{nom} - BR^{-1}B^T(\Pi(x_{nom})x_{nom} + s) \end{cases} \tag{16}$$

with $x_{nom}(0) = x_0$ and $s(T_f, x_{nom}(T_f)) = 0$, (see [20] for details).

The SDRE (15) is solved using a power series approximation. We begin by splitting A into a constant part and a state-dependent part as $A(x) = A_0 + \varepsilon g(x)\Delta A_C$, where ε is a temporary variable used for the expansion that will be set to 1 later. We next write Π as a power series in ε, as

$$\Pi(x,\varepsilon) = \sum_{n=0}^{\infty} \varepsilon^n g^n(x)(L_n)_C, \tag{17}$$

where Π as well as each $(L_n)_C$ is symmetric. Substituting these expansions into the state-dependent Riccati equation (15) and matching terms with the same powers of ε we obtain the following set of equations for determining the constant-valued matrices $(L_n)_C$:

$$(L_0)_CA_0 + A_0^T(L_0)_C - (L_0)_CBR^{-1}B^T(L_0)_C + Q = 0 \tag{18}$$

$$(L_1)_C\left(A_0 - BR^{-1}B^T(L_0)_C\right) + \left(A_0^T - (L_0)_CBR^{-1}B^T\right)(L_1)_C + (L_0)_C\Delta A_C + \Delta A_C^T(L_0)_C = 0 \tag{19}$$

$$(L_n)_C\left(A_0 - BR^{-1}B^T(L_0)_C\right) + \left(A_0^T - (L_0)_CBR^{-1}B^T\right)(L_n)_C + (L_{n-1})_C\Delta A_C + \Delta A_C^T(L_{n-1})_C - \sum_{k=1}^{n-1}\left((L_k)_CBR^{-1}B^T(L_{n-k})_C\right) = 0. \tag{20}$$

Equation (18) is the standard Riccati equation for the linear part of the system, A_0, which can be solved easily. Equations (19) and (20) are constant-valued matrix Lyapunov equations, for which stable and efficient algorithms also exist in the literature.

4.2. State Estimation for Nonlinear Systems

We consider a nonlinear control system with a nonlinear measurement of the form

$$\begin{cases} \dot{x}(t) &= f(x(t)) + Bu(x_e(t),t) \\ z(t) &= c(x(t)). \end{cases}$$

The control for a tracking problem is given by

$$u(x_e,t) = -R^{-1}B^T\left(\Pi(x_e)x_e + s(t,x_{nom})\right)$$

as discussed in the last section except now in terms of the estimated state x_e.

The estimated state will be formulated by an ordinary differential equation similar to the state equation, with a gain matrix (found using a dual state-dependent Riccati equation) applied to the difference between the measurements of the actual and estimated states. The coupled actual and estimated states are given by

$$\left\{ \begin{array}{rcl} \dot{x} & = & A(x)x - BR^{-1}B^T \left[\Pi(x_e)x_e + s(t, x_{nom})\right] \\ \dot{x}_e & = & A(x_e)x_e - BR^{-1}B^T \left[\Pi(x_e)x_e + s(t, x_{nom})\right] \\ & & + L(x_e)\left[z - c(x_e)\right], \end{array} \right. \tag{21}$$

where the state estimation gain is found by

$$L(x_e) = \Sigma(x_e)(C_0)^T V^{-1} \tag{22}$$

with $\Sigma(x_e)$ is the solution to the dual state-dependent Riccati equation

$$\Sigma(x_e)A^T(x_e) + A(x_e)\Sigma(x_e) - \Sigma(x_e)(C_0)^T V^{-1} C_0 \Sigma(x_e) + U = 0. \tag{23}$$

For the purposes of finding the estimator gain in equations (22)-(23) the nonlinear measurement function $z(t) = c(x(t))$ is rewritten as matrix function multiplication $c(x) = C(x)x$ and to choose $C_0 = C(0)$. We note that the nonlinearity of the measurement function does remain in the estimator system (21) itself, and the nonlinearity of the system dynamics remains in (21)-(23). The estimator gain SDRE (23) is solved using the power series approximation in an analogous fashion as described in previous section.

4.3. A Flight Dynamics Example

We apply the nonlinear estimator and feedback tracking control presented in previous sections to the flight dynamics example from [21]. The control system is given by

$$\dot{x} = \left(A_0 + x_2 A_{NL}\right) x + Bu, \qquad z(t) = [x_1, x_2, x_5]^T$$

where the matrices A_0, A_{NL} and B are given by:

$$A_0 = \begin{bmatrix} -0.0443 & 1.1280 & 0.0 & -0.0981 & 0.0 \\ -0.0490 & -2.5390 & 1.0 & 0.0 & -0.0854 \\ -0.0730 & 19.3200 & -2.2700 & 0.0 & 22.6834 \\ 0.0490 & 2.5390 & 0.0 & 0.0 & 0.0854 \\ 0.0 & 0.0 & 0.0 & 0.0 & 20.0 \end{bmatrix}$$

$$A_{NL} = \begin{bmatrix} -0.2317 & 0.0 & 0.0 & 0.0 & 0.0 \\ -1.2760 & -0.7922 & 0.0 & 0.0 & 0.0206 \\ 0.1020 & 64.2940 & -13.9710 & 0.0 & -5.4167 \\ 1.2760 & 0.7922 & 0.0 & 0.0 & -0.0206 \\ 0.0 & 0.0 & 0.0 & 0.0 & 0.0 \end{bmatrix}$$

$$B = \begin{bmatrix} 0.0 & 0.0 & 0.0 & 0.0 & 20.0 \end{bmatrix}^T.$$

The cost functional to be minimized is

$$J(x_0, u) = \frac{1}{2}\int_0^\infty \left((y - r)^T Q(y - r) + u^T R u\right) dt,$$

The state variables in this model represent the flight conditions of the aircraft: x_1 is the deviation of the velocity from the level flight trim value of 1(100m/s) (given in units of (100m/s)), x_2 is the deviation of the angle of attack from the trim value of $4.2(\pi/180)$ radians, x_3 is the pitch rate in rad/s, x_4 is the flight path angle in radians, and x_5 is the deviation of the canard deflection angle in radians from the trim value, which is not given. The control u is the input canard deflection in radians. The canards are control flaps which can deflect downward by up to $90(\pi/180)$ radians. Finally, $y(t) = x_4(t)$ is the tracking flight path angle and $r(t)$ is the desired flight path angle.

The weights are $Q = 1$, $R = 1$, $U = 100I_5$ and $V = I_3$. The actual state starts at the origin, but the estimated state starts slightly off the actual, at $(x_e)_0 = (0, 0, 0, 5(\pi/180), 0)^T$. Figure 4 depicts the estimated state almost converging to the actual state by the time of the desired x_4 increase, and remaining close to the actual state for the rest of the time period. In Figure 5 we plot the actual

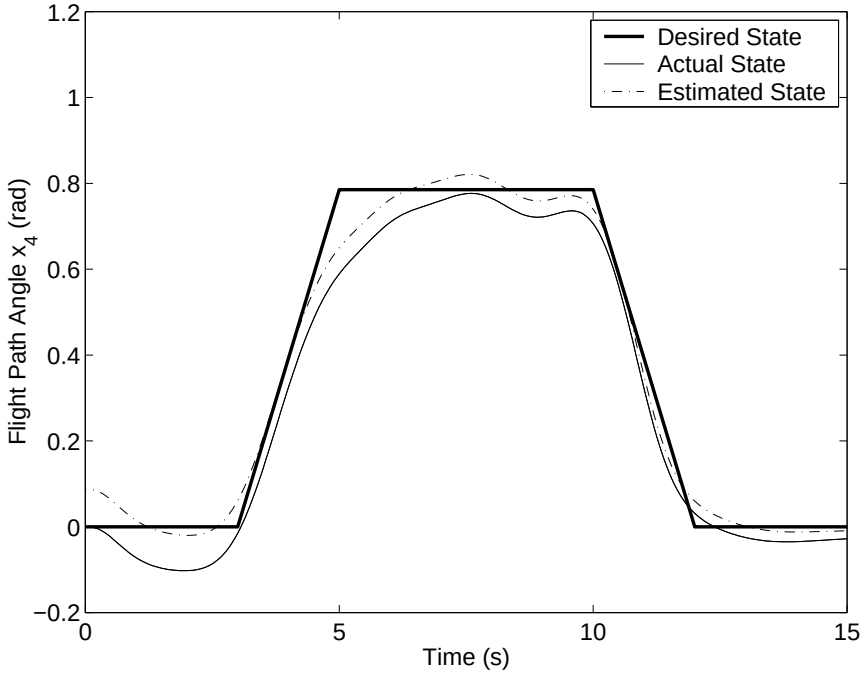

FIGURE 4. Actual and estimated states for nonlinear tracking control/state estimator

state when controlled using our fully nonlinear algorithm, as well as when using the linear SE gain control (as proposed in [22]), and the fully linearized control. It can be seen that the linear control overshoots significantly at the top of the ascent

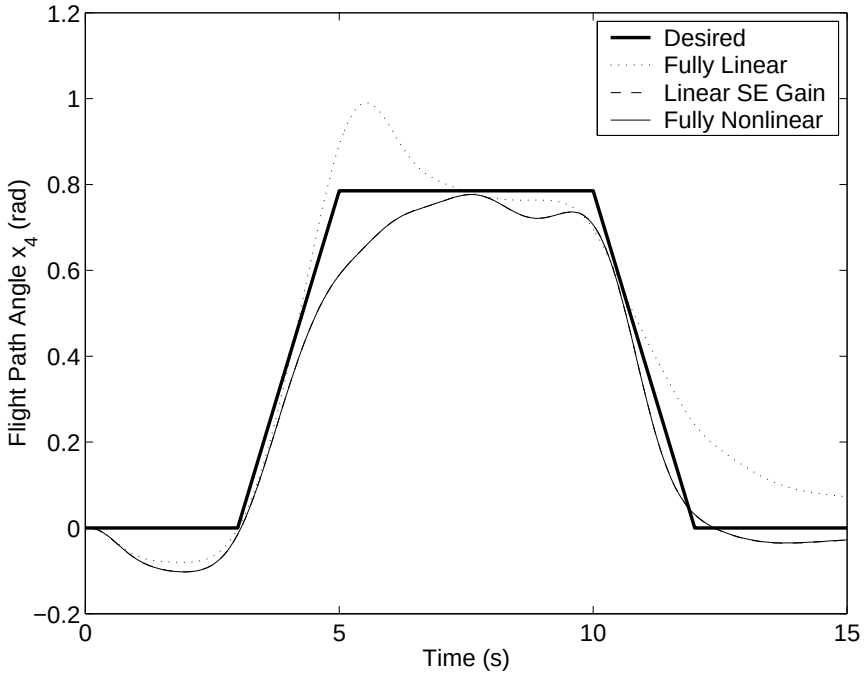

FIGURE 5. Comparison of tracking controls/state estimators with inaccurate $(x_e)_0$.

and is very slow to return to 0. The other two methods produce virtually identical results (the difference is indiscernable in the plots in Figure 5).

In the recent manuscript [23], we have successfully applied these methodologies to feedback tracking control of the GaP film thickness in a high-pressure CVD reactor that is more complex and realistic than the one presented here. Some of the complexities that were considered in [23] include 3-dimensional flow region, 10 atm operating condition, multiple species that include gas-phase kinetics as well as nonlinear surface kinetics, and nonlinear partial state observation.

5. Conclusions

In this paper we report on the development of nonlinear compensators and nonlinear feedback tracking control methodologies that can be applied to high pressure CVD systems. We also present successful computational implementation of reduced order feedback control of pulsed high pressure CVD III-V film growth involving the transport of multiple species with linear gas phase reactions. The combination of reduced order model methods based on proper orthogonal decomposition techniques with nonlinear compensator-based feedback tracking control

can provide a powerful tool for treating more complex situations that may be encountered when nonlinear gas phase and/or nonlinear surface phase reactions are present.

6. Acknowledgements

This research was supported in part by a DOD/AFOSR MURI Grant AFOSR F49620-95-1-0447, in part by the AFOSR under Grant F49620-98-1-0180, and in part by the AFOSR under Grant F49620-96-1-0292 (AASERT).

References

[1] D. Olego, *Status and projections of blue light emitters,* Plenary Lecture, TMS Electronic Materials Conference, June 22, 1994.

[2] K. Fukunaga, *Introduction to Statistical Pattern Recognition*, (1972), Academic Press, New York.

[3] G. Berkooz, P. Holmes and J.L. Lumley, *The proper orthogonal decomposition in the analysis of turbulent flows*, Annual Review of Fluids Mechanics, **25** (1993), N5:539–575.

[4] G. Berkooz, P. Holmes, J.L. Lumley and J.C. Mattingly, *Low-dimensional models of coherent structures in turbulence*, Physics Reports-Review Section of Physics Letters, **287** (1997), N4:338–384.

[5] M. Rajaee, S.K.F. Karlson and L. Sirovich, *Low-dimensional description of free-shear-flow coherent structures and their dynamical behavior*, J. of Fluid Mechanics, **258** (1994), 1–29.

[6] M. Kirby and L. Sirovich, *Application of the Karhunen-Loève procedure for the characterization of human faces*, IEEE Trans. on Pattern Analysis and Machine Intelligence, **12** (1990), N1:103–108.

[7] R. Hilai and J. Rubinstein, *Recognition of rotated images by invariant Karhunen-Loève expansion*, J. of the Optical Society of America A-Optics Image Science and Vision, **11** (1994), N5:1610–1618.

[8] H.V. Ly and H.T. Tran, *Proper orthogonal decomposition for flow calculations and optimal control in a horizontal CVD reactor*, CRSC Tech. Report **98-13** (1998), North Carolina State University, Raleigh, North Carolina; Quarterly of Applied Mathematics, to appear.

[9] H.V. Ly and H.T. Tran, *Modeling and control of physical processes using proper orthogonal decomposition*, Computers and Mathematics with Applications, to appear.

[10] C. Theodoropolous, R.A. Adomaitis and E. Zafiriou, *Model reduction for optimization of rapid thermal chemical vapor deposition systems*, IEEE Trans. Semiconductor Manufacturing, **11** (1998), 85–98.

[11] G.M. Kepler, H.T. Tran and H.T. Banks, *Reduced order model compensator control of species transport in a CVD reactor*, CRSC Tech. Report **99-15** (1999), North Carolina State University, Raleigh, North Carolina; Optimal Control Applications and Methods, to appear.

[12] G.M Kepler, H.T. Tran and H.T. Banks, *Compensator control for chemical vapor deposition film growth using reduced order design models*, CRSC Tech. Report **99-41** (1999), North Carolina State University, Raleigh, North Carolina; IEEE Trans. on Semiconductors, to appear.

[13] H.T. Banks, R.C.H. del Rosario and R.C. Smith, *Reduced order model feedback control design: Numerical implementation in a thin shell model*, CRSC Tech. Report **98-27** (1999), North Carolina State University, Raleigh, North Carolina; IEEE Trans. on Aut. Control, to appear.

[14] K. Kunisch and S. Volkwein, *Control of Burgers' equation by a reduced order approach using proper orthogonal decomposition*, Optimierung und Kontrolle Bericht **138** (1998), Universitat Graz, Austria; J. Opt. Theory Applic., to appear.

[15] J.A. Atwell and B. King, *Proper orthogonal decomposition for reduced basis feedback controllers for parabolic equation*, ICAM Report **99-01-01** (1999), VPISU, Blacksburg, Virginia; Math. and Comp. Modeling, to appear.

[16] H.T. Banks, M.L. Joyner, B. Wincheski and W.P. Winfree, *Nondestructive Evaluation using reduced-order computational methodology*, Inverse Problems, **16** (2000), 929–945.

[17] K.J. Bachmann, N. Sukidi, C. Hopfner, C. Harris, N. Dietz, H.T. Tran, S. Beeler, K. Ito and H.T. Banks, *Real-time monitoring of steady-state pulsed chemical beam epitaxy by p-polarized reflectance,* J. of Crystal Growth, **183** (1998), 323–337.

[18] C. Theodoropolous, N.K. Ingle, T.J. Mountziaris, Z.Y. Chen, P.L. Liu, G. Kioseoglou and A. Petrou, *Kinetic and transport modeling of the metallorganic chemical vapor deposition of InP from trimethylindium,* J. Electrochem. Soc., **142** (1995), 2086–2094.

[19] S. Beeler, H.T. Tran and N. Dietz, *Representation of GaP formation by a reduced order surface kinetics model using p-polarized reflectance measurements,* J. of Applied Physics, **86** (1999), 674–682.

[20] S. Beeler, H.T. Tran and H.T. Banks, *State estimation and tracking control of nonlinear dynamical systems*, CRSC Tech. Report **00-19** (2000), North Carolina State University, Raleigh, North Carolina; Automatica, submitted.

[21] W.L. Garrard, D.F. Enns and S.A. Snell, *Nonlinear feedback control of a highly maneuvrable aircraft,* Int. J. of Control, **56** (1992), 799–812.

[22] F.E. Thau, *Observing the state of non-linear dynamic systems,* Int. J. of Control, **17** (1973), 471–479.

[23] S.C. Beeler, G.M. Kepler, H.T. Tran and H.T. Banks, *Reduced order modeling and control of thin film growth in an HPCVD reactor*, CRSC Tech. Report **00-33** (2000), North Carolina State University, Raleigh, North Carolina.

Center for Research in Scientific Computation,
Department of Mathematics,
North Carolina State University,
Raleigh, North Carolina 27695
E-mail address: htbanks@eos.ncsu.edu; tran@control.math.ncsu.edu